CILAMCE 2017
Florianópolis - Santa Catarina - Brazil

ANALYSIS OF RATE EFFECTS INDUCED BY CAVITY EXPANSION IN SILTY SOILS USING A DRUCKER-PRAGER CAP PLASTICITY MODEL

Gracieli Dienstmann

g.dienstmann@gmail.com

Department of Civil Engineering, Federal University of Santa Catarina

Rua João Pio Duarte da Silva, 205 – Córrego Grande, 88037-000, Florianópolis, Brasil

Fernando Schnaid

Samir Maghous

fschnaid@gmail.com

samir.maghous@ufrgs.br

Department of Civil Engineering, Federal University of Rio Grande do Sul

Avenida Osvaldo Aranha, 99 - Centro Histórico, 90035-190, Porto Alegre, Brasil

Abstract. *The drainage conditions during cone penetration tests is a critical factor in the assessment of tailings properties, since they often involve materials with permeability ranging from 10^{-5} to 10^{-8} m/s, which are typical values for silty soils. In such materials, a partially drainage behavior is likely to occur during the standard penetration test, which leads to errors in interpretation. Aiming to understand the processes that control the drainage behavior during penetration, a simplified model was formulated in Dienstmann et al. (2017). The model provides semi-analytical solutions for pore-fluid pressure, displacement and stress distributions around an expanding rigid infinite cylinder embedded within a saturated porous medium. The poromechanic approach is based on the local equivalence between the response of a perfectly plastic behavior to the monotonic loading process and an appropriate fictitious nonlinear poroelastic behavior. A Drucker Prager yield condition is adopted in the formulation. In the present work, results of the model predictions are directly compared with poroplastic finite element solutions using both a Drucker-Prager and Drucker-Prager Cap plasticity models. The analysis allows to quantitatively discuss the impact on the model predictions, as well as their correlation with the drainage conditions, when a cap is introduced to limit the domain of elastic compressive stresses. Useful recommendations for interpretation and analysis of in situ measured properties will be formulated in light of the present study.*

Keywords: *expanding cylinder, Non-linear poroelasticity, Porous medium, Transient flow, Finite element analysis.*

1 INDRODUCTION

Countries with large mining industry operations face serious environmental responsibilities emerging from large-scale mining operations, tailings dam incidents and occasional dam failures. The design of tailings storage facilities (TSF) is still a challenge to geotechnical engineers because of the high complexity involving the tailings geotechnical behavior coming from the heterogeneous nature of waste products, the hydraulic depositional processes and the change in the constitutive parameters during the lifetime of deposits.

The experience gathered in the last 20 years (e.g. Schnaid et al. 2013 Jamiolkowsky & Masella, 2014) shows that the depositional process often produces tailings in the so-called intermediate permeability range of 10^{-5} to 10^{-8} m/s. In intermediate soils, including natural clayey and sandy–silts, tailing and others geomaterials, a partially drainage behavior is likely to occur when *in situ* tests as cone penetration are performed at the standardized velocity (20mm/s), introducing errors in interpretation.

In this context, theoretical solutions can be an essential tool helping understanding what controls the drainage behavior taking place during cone penetration tests executed in silty materials. Among the existing methods, cavity expansion approach is extensively used and accepted for modeling the cone penetration (e.g. Gibson and Anderson, 1961; Baligh, 1985; Teh and Houlsby, 1991; Yu and Mitchell, 1998; Burns and Mayne, 2000; Chang et al. 2001; Cao et al., 2001; Chen and Abousleiman, 2012, 2013; Zhang et al., 2016), with a variety of soil stress–strain models. Although, there is an extensively literature on cavity expansion solutions applied to the interpretation of piezocone tests, there is not a complete understanding of what controls the transient behavior during penetration.

Aiming to understand the processes that control the drainage behavior during penetration, a simplified model was formulated in Dienstmann et al. (2017). The model provides semi-analytical solutions for pore-fluid pressure, displacement and stress distributions around an expanding rigid infinite cylinder embedded within a saturated porous medium. The developed solution, which considers a Drucker Prager yield condition, will be briefly described in the present paper and results of the model predictions will be directly compared with poroplastic finite element solutions using both a Drucker-Prager and Drucker-Prager Cap plasticity models. The intention is to quantitatively discuss the impact on the model predictions, as well as their correlation with the drainage conditions, when a cap is introduced to limit the domain of elastic compressive stresses.

In all what follows, the sign convention of positive stress values for tension and negative stress values for compression will be adopted.

2 MODEL DESCRIPTION

The cylindrical cavity expansion problem is structured as a consolidation analysis of a rigid cylinder deeply embedded within an isotropic fully saturated medium of infinite extent. The analysis is based on the assumption of plane strain conditions in the cross-section of a system defined by the cylinder and surrounding porous medium, restricting displacements and flow to two dimensions (Figure 1).

Proceedings of the XXXVIII Iberian Latin-American Congress on Computational Methods in Engineering
P.O. Faria, R.H. Lopez, L.F.F. Miguel, W.J.S. Gomes, M. Noronha (Editores), ABMEC, Florianópolis, SC, Brazil, November 5-8, 2017.

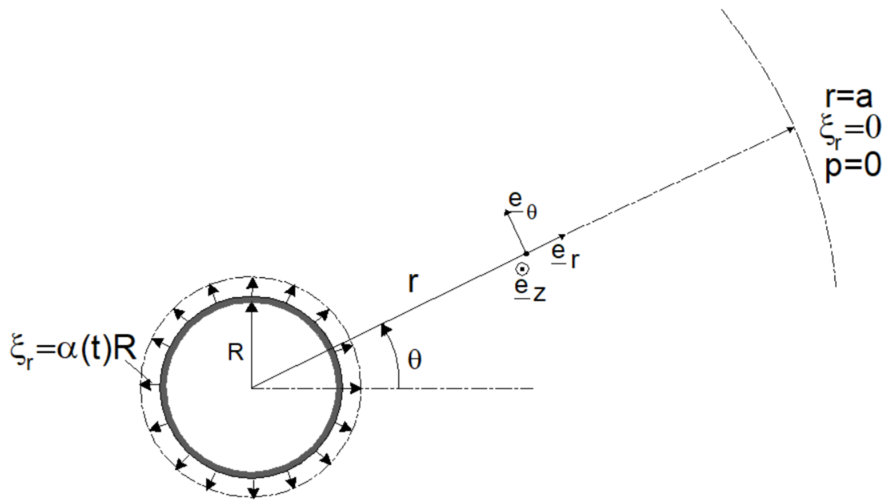

Figure 1. Idealized geometry and loading conditions for consolidation around infinite expanding cylinder.

Starting from an initial stress and pore pressure states (σ_0, p_0), a prescribed radial displacement of magnitude $\alpha(t)R$ is applied at the cylinder wall $r = R$. The concept of influence zone $R \le r \le a$ is also introduced in the analysis to characterize the extent of the region whose poromechanical state is no longer affected by cylinder installation and subsequent expansion (e.g. Blight, 1968; Randolph and Wroth, 1979; Osman and Randolph, 2012). This means in particular that displacement and pore pressure vanish at $r = a$. The cylinder geometry may be viewed as a simplest conceptual model of a pile, shield, shaft or piezocone test, and the associated solution would then be relevant to the consolidation of soil around the cylinder induced by its expansion during related *in situ* test.

2.1 Analytical cylindrical cavity expansion solution

A constitutive model based on the local equivalence between the response of a perfectly plastic behavior to monotonic loading process and an appropriate fictitious non-linear poroelastic behavior has been formulated in Dienstmann et al. (2017) to analyze the consolidation and rate effects induced by the expansion of a rigid cylinder embedded within an isotropic elastic medium of infinite extent (Fig. 1). The theoretical features of the model, whose detailed description may be found in Dienstmann et al. (2017), shall be briefly recalled in the sequel. For the sake of simplicity, the reference state is defined by null initial stress and pore pressure (i.e., $\sigma_0 = p_0 = 0$). The extension to non-zero initial state can be found in the original work.

From a purely phenomenological viewpoint, the poro-elastoplastic behavior of medium under monotonic loading can be represented by means of a non-linear poroelastic material involving secant stiffness parameters. The starting idea is then to relate stress $\boldsymbol{\sigma}$ to skeleton strain $\boldsymbol{\varepsilon}$ and pore pressure p through non-linear first state poroelastic relationships

$$\boldsymbol{\sigma} = \mathbf{C} : \boldsymbol{\varepsilon} - b\, p \mathbf{1} \tag{1}$$

where $\mathbf{C} = \mathbf{C}(\boldsymbol{\varepsilon})$ is the tensor of drained (non-linear) elastic moduli, which is defined in the context of isotropy by the bulk modulus K and shear modulus G, and b is the Biot coefficient. The non-linear poroleastic behavior described by (1) is then conceived as an asymptotic representation of the plastic yield stress of the material. Let the latter be described by a yield function controlled by the value of the Terzaghi effective stress

$$F(\boldsymbol{\sigma}' = \boldsymbol{\sigma} + p\mathbf{1}) \leq 0 \tag{2}$$

Accordingly, the stress derived from (1) shall comply with:

$$\lim_{\varepsilon_d/\varepsilon_{ref} \to \infty} F(\boldsymbol{\sigma}' = \boldsymbol{\sigma} + p\mathbf{1}) = 0 \tag{3}$$

where ε_d is the equivalent deviatoric strain and $\varepsilon_{ref} << 1$ is a strain that physically represents the order of magnitude of the shear strain mobilized at yielding. Considering a Drucker-Prager yield condition for the material strength, it can be shown (Lemarchand et al., 2002; Maghous et al., 2009) that the secant shear modulus in the equivalent non-linear poroelastic constitutive law must comply with:

$$G(\varepsilon_d, \varepsilon_v, p) \approx \frac{1}{2\varepsilon_d}\left[T(h - K\varepsilon_v - (1-b)p)\right] \quad \text{when } \varepsilon_d / \varepsilon_{ref} >> 1 \tag{4}$$

In the above equation, parameters h and T respectively characterize the tensile strength and the friction coefficient of the medium. A comprehensive modeling of the non-linear behavior of the material would rely upon the identification of function $G(\varepsilon_d, \varepsilon_v, p)$ from experimental data. A simple way to meet the above condition consists in considering the following law:

$$G(\varepsilon_d, \varepsilon_v, p) = \frac{1}{2}\left[T(h - K\varepsilon_v - (1-b)p)\right] \times \frac{1/\varepsilon_{ref}}{1 + \varepsilon_d / \varepsilon_{ref}} \tag{5}$$

together with a constant value for the bulk modulus, K. The non-linear poroelastic behavior defined by (Eq. 5) is sketched in Figure 2.

The pore flow component of the solution follows a combination of the fluid mass balance equation, the second poroelastic state equation and Darcy´s law with

$$b\frac{\partial \varepsilon_v}{\partial t} + \frac{1}{M}\frac{\partial p}{\partial t} = k\nabla^2 p \tag{6}$$

where M is the material Biot modulus, and k is the permeability coefficient. From the classical reasoning to non-linear poroelastic medium, the following generalized Navier equation can be derived (assuming irrotational displacement field)

$$\left[K + \tfrac{4}{3}G\right]\nabla\varepsilon_v + 2\nabla G \cdot (\boldsymbol{\varepsilon} - \tfrac{1}{3}\varepsilon_v\mathbf{1}) = b\nabla p \tag{7}$$

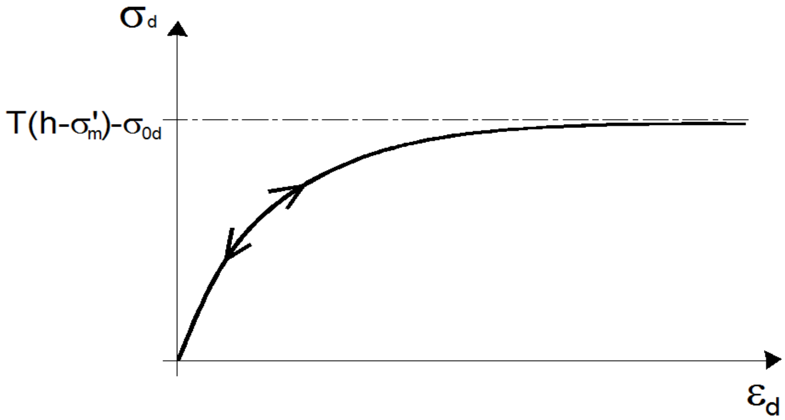

Figure 2. Representation of the non-linear elastic behavior associated with a Drucket-Prager yield condition.

The above equation emphasizes the strong coupling between skeleton strains and pore-fluid pressure. Unlike classical formulations in which only the volumetric part ε_v of skeleton strains affects pore-fluid pressure, the latter is also explicitly related to the deviatoric part $G(\varepsilon_d, \varepsilon_v, p)$ of skeleton strains through the shear modulus ε_d. In classical formulations considering a constant shear modulus, the volume strain ε_v is eliminated between Eqs. (6) and (7) to obtain an uncoupled pressure diffusion equation governing the evolution of pore pressure. Unfortunately, this is not possible due to dependence of the shear modulus on strains, and a specific procedure is then needed to solve the coupled problem.

As shown, the problem of consolidation around infinite expanding cylinder is idealized in Figure 1. Starting from an initial stress and pore pressure states (σ_0, p_0), a radial displacement of magnitude $\alpha(t)R$ is prescribed at the cylinder wall $r = R$. The solution to this idealized problem is sought in the form $f(r,t)\,\underline{\boldsymbol{e}}_r$ for the displacement distribution and $p(r,t)$ for the pore pressure distribution. Determination of the pore pressure distribution $p(r,t)$ and displacement function $f(r,t)$ requires solving the coupled system defined by the set of non-linear partial differential equations (6) and (7), together with associated boundary and initial conditions. A time incremental procedure has been implemented in Dienstmann et. al (2017) to access semi-analytical solutions to this problem. The approach makes use of a specific iterative algorithm within each time step.

Initial excess pore-fluid pressure distribution

Most expressions proposed in literature for the initial excess of pore pressure u_0 (or equivalently p_0) generated by insertion of a rigid cylinder within the medium, have been based on laboratory or field data. However, none of these expressions actually comply with the condition of null fluid flow at the cylinder wall. In this regards, a new expression has been

Proceedings of the XXXVIII Iberian Latin-American Congress on Computational Methods in Engineering
P.O. Faria, R.H. Lopez, L.F.F. Miguel, W.J.S. Gomes, M. Noronha (Editores), ABMEC, Florianópolis, SC, Brazil, November 5-8, 2017.

proposed in Dienstmann et al. (2017). It extends classical expressions to account for the flow restriction at cylinder wall:

$$u_0(r) = u_{0,\max} \frac{\mathfrak{F}(r)}{\mathfrak{F}(R)} \quad \text{whit} \quad \mathfrak{F}(r) = 1 - \frac{a_0}{r} + \frac{a_0}{R} \ln \frac{a_0}{r} \quad \text{for } R \le r \le a_0 \tag{8}$$

Where $u_{0,\max}$ refers to the maximum value of pore pressure generated by cylinder insertion. In the present paper $u_{0,\max}$ is estimated by the pore pressure generated during consolidation phase in an undrained triaxial test

$$u_{0,\max} = \frac{p_{c0}}{2}\left(1 + M_{cs}\right) \tag{9}$$

where p_{c0} denotes a reference initial consolidation pressure, and M_{cs} is the slope of the critical state line.

Parameter a_0 in Eq. 8 characterizes the distance beyond which the initial excess pore pressure becomes negligibly small.

2.2 Drucker Prager and Modified Drucker Prager – CAP model

This subitem briefly describes the Drucker Prager and Modified Drucker Prager Cap plasticity models available in the finite element software ABAQUS.

Drucker Prager plasticity model

According ABAQUS (2009) the extended Drucker-Prager models are used to model frictional materials, which are typically granular-like soils and rock, and exhibit pressure-dependent yield. The yield criteria for this class of models are based on the shape of the yield surface in the meridional plane, which can assume a linear form according Figure 3 (a). In this case the Drucker–Prager failure surface is given by:

$$F_S = t - p \tan\beta - d \tag{10}$$

where

β - is the slope of the linear surface in $p - t$ stress plane and is commonly referred to as the friction angle of the material;

d - is the cohesion of the material; and t is given by:

$$t = \frac{1}{2} q \left[1 + \frac{1}{K_{DP}} - \left(1 - \frac{1}{K_{DP}}\right)\left(\frac{r}{q}\right)^3 \right] \tag{11}$$

where

K_{DP} - is the ratio of yield stress in triaxial tension to the yield stress in triaxial compression, and controls the dependence of the yield surface on the value of intermediate principal stress, Figure 3(c). When $K_{DP} = 1$, $t = q$, which implies that the yield surface is the Von Mises circle in the deviatoric principal stress plane, in which case the yield stresses in triaxial tension and compression are the same;

p - is the equivalent pressure stress: $p = -\frac{1}{3} tr\boldsymbol{\sigma}$;

q - is the Mises equivalent stress: $q = \sqrt{\frac{2}{3}\mathbf{S}:\mathbf{S}}$;

$\mathbf{S}$ - is the stress deviator: $\mathbf{S} = \boldsymbol{\sigma} - p\mathbf{1}$

r - is the third invariant of deviatoric stress: $r = \left(\frac{9}{2}\mathbf{S}:\mathbf{S}:\mathbf{S}\right)^{1/3}$

A plastic flow rule is given by the flow potential:

$$G_{flow} = t - p\tan\psi \tag{12}$$

where ψ is a dilation angle in the $p - t$ plane. Figure 3 (b) shows the hardening low applied in $p - t$ space.

Elastic behavior in Drucker Prager plasticity model can be modeled as linear elastic using the generalized Hooke's law (E - Young Modulus, ν - Poisson Ratio) or as a porous elastic material. Porous elasticity in Abaqus is a non-linear, isotropic model in which the pressure stress varies as an exponential function of volumetric strains. In all further F.E. analysis, the linear elastic behavior will be adopted.

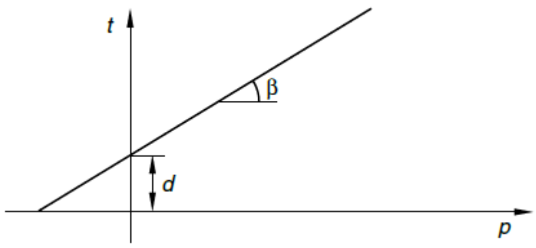

(a)

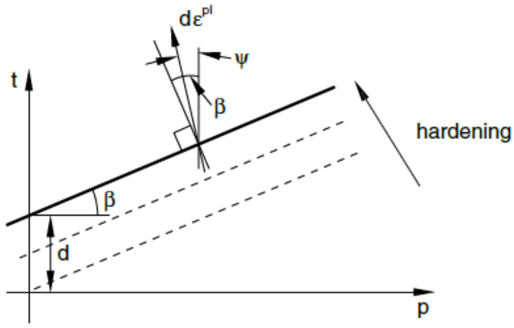

(b)

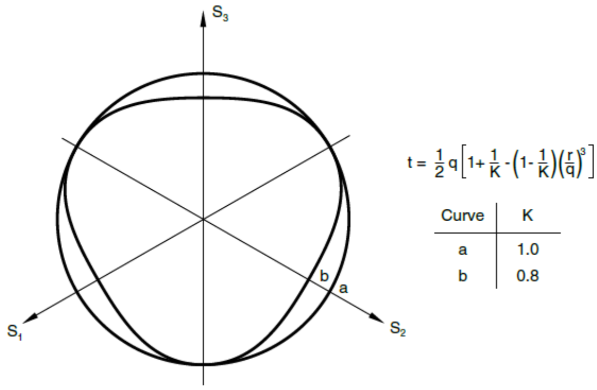

(c)

Figure 3. Drucker-Prager model: (a) Linear Yield surfaces in the meridional plane; (b) Linear Drucker-Prager model: yield surface and flow direction in the p–t plane. (c) Typical yield/flow surfaces of the linear model in the deviatoric plane.

Modified Drucker Prager Cap plasticity model

The yield surface of the modified Drucker Prager Cap plasticity model consists of three parts: a Drucker–Prager shear failure surface (F_s), an elliptical cap surface (F_c), which intersects the mean effective stress axis at a right angle, and a smooth transition region between the shear failure surface and the cap (F_t), as shown in Fig. 4. Elastic behavior in Drucker Prager Cap model can also be modeled as linear elastic using the generalized Hooke's law, or as porous elastic. The onset of plastic behavior is determined by the Drucker–Prager failure surface and the cap yield surface. The Drucker Prager failure surface is given by Eq. 10.

Proceedings of the XXXVIII Iberian Latin-American Congress on Computational Methods in Engineering
P.O. Faria, R.H. Lopez, L.F.F. Miguel, W.J.S. Gomes, M. Noronha (Editores), ABMEC, Florianópolis, SC, Brazil, November 5-8, 2017.

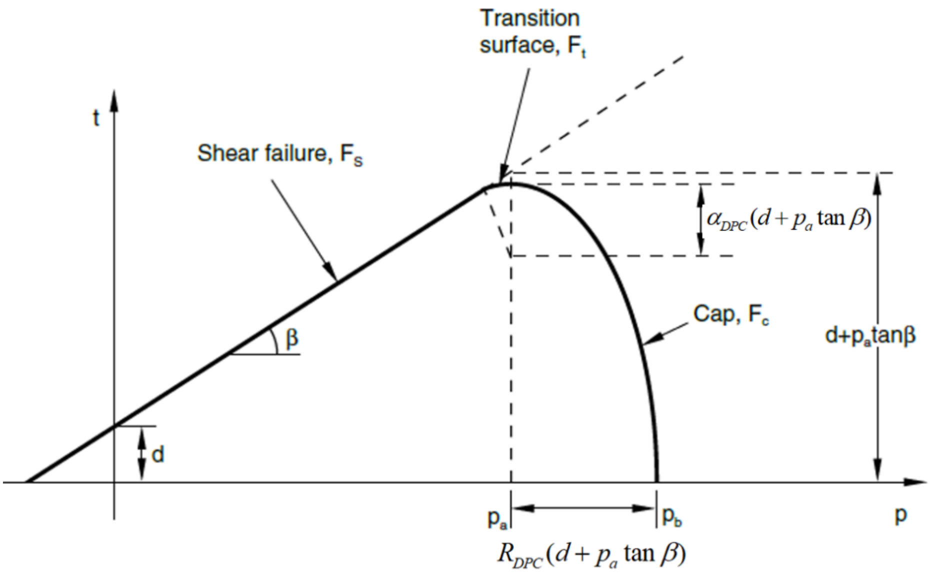

Figure 4. Drucker-Prager CAP model

The cap surface hardens (expands) or softens (shrinks) as a function of the volumetric plastic strain. The cap yield surface is given as:

$$F_c = \sqrt{[p-p_a]^2 + \left[\frac{R_{DPC}t}{1+\alpha_{DPC}-\alpha_{DPC}/\cos\beta}\right]^2} - R_{DPC}(d+p_a\tan\beta) = 0 \tag{13}$$

where R_{DPC} is a material parameter that controls the shape of the cap, and α_{DPC} is a small number, typically around 0.01 to 0.05 used to define a smooth transition surface between the Drucker Prager Shear surface and the cap:

$$F_t = \sqrt{[p-p_a]^2 + \left[t + \left(1-\frac{\alpha_{DPC}}{\cos\beta}(d+p_a\tan\beta)\right)\right]^2} - \alpha_{DPC}(d+p_a\tan\beta) = 0 \tag{14}$$

in where p_a is an evolution parameter that controls the hardening-softening behavior as a function of the volumetric plastic strain:

$$p_a = \frac{p_b - R_{DPC}d}{(1+R\tan\beta)} \tag{15}$$

with p_b the mean effective (yield) stress.

p_b is a user-defined piecewise linear function relating the evolution of the mean effective stress with the volumetric inelastic strain ε_{vol}^{pl} according Fig. 5.

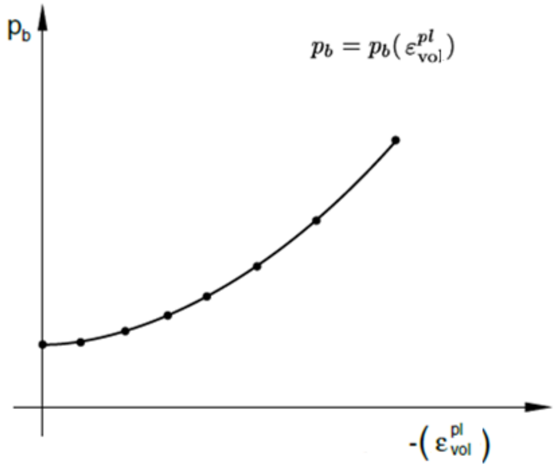

Figure 5. Typical cap hardening

Conventionally, the hardening curve (Fig. 5) can be obtained from the isotropic consolidation test results:

$$\varepsilon^{pl}_{vol} = \frac{\lambda - \kappa}{(1+e_0)} \ln \frac{p_b}{p_{b0}} \tag{16}$$

Where λ is the compression index, κ is the recompression index, e_0 is the initial void ratio, and p_{b0} in the initial mean effective stress.

3 NUMERICAL ANALYSIS

The simplified model developed for consolidation around an expanding cylinder has been formulated within the framework of non-linear poroelasticity, extending the concept of deformation (or Henky) plasticity to porous media. The semi-analytical solution for pore-fluid pressure, stress and displacement fields induced by cylinder expansion can be fully accessed in Dienstmann et al. (2017). In the present section, results of the model predictions are directly compared with poroplastic finite element solutions using both a Drucker-Prager and Drucker-Prager Cap plasticity models. The analysis allows to quantitatively discuss the impact on the model predictions, as well as their correlation with the drainage conditions, when a cap is introduced to limit the domain of elastic compressive stresses.

For the finite element (F.E.) analysis the consolidation problem induced by cylinder expansion (Fig.1) is treated as a plane strain axisymmetric problem in a plane normal to the vertical direction. The discretized mesh is defined by a “slice” of the porous medium with appropriate mechanical boundary conditions as sketched in Figure 6. The extension of the slice is set to100R ($a = 100 \times R$), which proved sufficient to simulate boundary conditions at infinity (i.e. at $r >> R$).

Proceedings of the XXXVIII Iberian Latin-American Congress on Computational Methods in Engineering
P.O. Faria, R.H. Lopez, L.F.F. Miguel, W.J.S. Gomes, M. Noronha (Editores), ABMEC, Florianópolis, SC, Brazil, November 5-8, 2017.

The finite element grid consists in quadrilateral 8-node elements (CAX8RP), with piecewise quadratic approximation for displacement, piecewise linear approximation for pore pressure and reduced integration elements. Size and dimensions of the finite element mesh were selected from preliminary mesh sensitivity (convergence) analysis based on different spatial discretization of geometry domain. The adopted mesh consists in a slice discretized into 1100 quadrilateral elements, corresponding to 13208 degrees of freedom (nodal values of displacement and pore pressure). The size of element is $0.01R$ at the cavity wall and increases according to a bias ratio of 25 in the $R \le r \le a_0$ range, while in the $r > a_0$ domain the elements are regularly distributed.

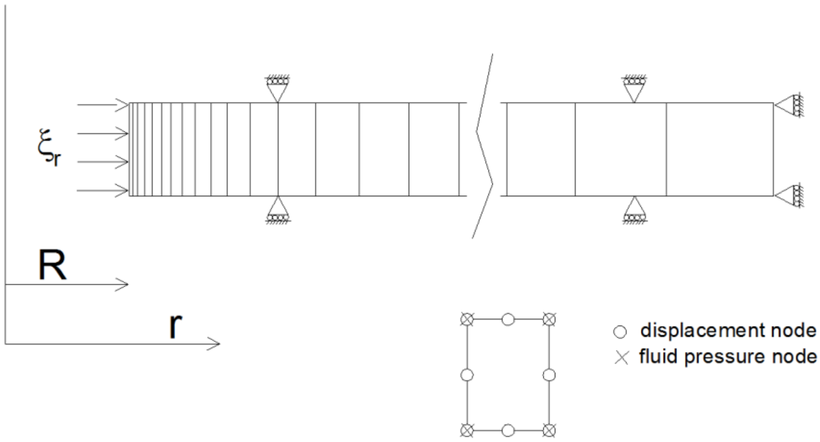

Figure 6. Finite element model

For the present study two sets of parameters are evaluated varying G_0 [$G_0 = G(\varepsilon_d = 0, \varepsilon_v = 0, p = p_0)$], initial shear modulus. The selected parameters used are summarized in Tables 1 to 3. An isotropic and uniform (in the plane of analysis) stress field $\boldsymbol{\sigma}_0 = -\sigma_0 \mathbf{1}$ is adopted in all further analysis, with an initial field of excess pore-fluid pressure $u_0(r)$ calculated from equation (8), considering $a_0 = 50R$. As regards the initial cavity radius a conventional 10 cm^2 piezocone cross-section was considered, representing an initial radius $R = 0.0178\,\text{m}$.

Constant values of T, frictional parameter and h cohesion are adopted in the analysis. Expressions correlating the frictional parameters (β and T) and cohesion (h and d) are given by:

$$\tan\beta = T\frac{\sqrt{6}}{2} \tag{17}$$

$$d = h.\tan\beta \tag{18}$$

A constant value of poisson ratio of 0.3 was used to derive the Bulk Modulus (K), and Young Modulus (E) of the soil matrix. References values of K_s (Bulk modulus of the solid phase - solid grains) and K_w (Bulk Modulus of the fluid phase) are used in the analysis, from those we obtain the Biot coefficient (b), Biot Modulus (M) and coefficient of diffusivity (c_f)

The dilatancy angle required for definition of the Drucker Prager poroplastic model that is adopted for the ABAQUS has been fixed to $\psi = 0^o$.

Additionally, for Drucker Prager models parameter K_{DP} - ratio of yield stress in triaxial tension to the yield stress in triaxial compression - was set as unity. Cap parameters: R_{DPC} is also set as unity; and α_{DPC}, parameter that controls the transitional surface shape was defined as 0 (zero), which means that no transitional surface is considered. For the cap hardening reference values of $\lambda = 0.1$ and $\kappa = 0.01$ were adopted.

It is important to highlight that the adopted set of parameters (Table 1 to 3) are part of a preliminary sensitivity analysis. Complementary analyzes varying cap model parameters as R_{DPC}, α_{DPC} and p_b would be addressed in future works.

Table 1: common properties

Comum properties		
e_0	1.2	Initial void ratio
k (m/s)	1E-08	Permeability
$u_{0,\max}$ (kPa)	100	Initial excess pore pressure
σ_0 (kPa)	150	Initial stress

Table 2: Semi-analytical model

Semi-analytical Model											
Case	G_0 (kPa)	T	h (kPa)	ε_{ref}	ν	K (kPa)	K_s (kPa)	K_w (kPa)	b	M (kPa)	c_f (m/s)
1	500	0.9838	1	0.0510	0.30	1083	100000	2200000	0.99	213444	1.77E-06
2	2500	0.9838	1	0.0103	0.30	5416	100000	2200000	0.95	235199	9.40E-06

Table 3: Drucker Prager Plasticity models

Drucker Prager and Drucker Prager CAP								**Drucker Prager CAP**			
Case	ν	E	c_f (m/s)	β	d (kPa)	ψ	K_{DP}	R_{DPC}	α_{DPC}	κ	λ
1	0.30	1300	2.08E-06	50.5	1.21	0	1	1	0	0.01	0.1
2	0.30	6500	9.99E-06	50.5	1.21	0	1	1	0	0.01	0.1

The loading process is defined by increasing the prescribed displacement applied to the cylinder wall from zero to a maximum value of $0.1R$, the goal is to keep deviator strains ε_d (deviatoric strain) around 10%. Three typical values for expansion rates are investigated in the analysis. They range from $V = 10^{-5}$ mm/s which is characteristic of drained evolution of the porous medium during the test, to $v = 10^{-3}$ mm/s for partially drained evolution, and $v = 1$ mm/s that is considered to be representative of undrained response of the soil surrounding the expanding cylinder. Results from the numerical simulations together with the analytical predictions are sketched in Figures 7 to 12.

Referring to the results shown in Figures 7(a) and 7(b), when $G_0 = 500kPa$, Case 1, it can be observed that the maximum increment on radial effective stresses ($\Delta\sigma^{'}_{rr}$) and pore pressure (p) are very sensitive to the expansion rate. The non-linear poroelastic model and both poroplastic F.E. solutions predict decreasing values for the maximum stress as the expansion rate increases, passing from the fully drained regime to undrained regime. F.E. solutions, Drucker Prager and Drucker Prager Cap models, predict slightly higher values of pore pressure, especially at the undrained behavior. A general agreement on $\Delta\sigma^{'}_{rr}$ is observed, except for the fastest velocity (1mm/s), undrained behavior. In this case the cap maximum values of $\Delta\sigma^{'}_{rr}$ are sensitively lower.

Figure 8 shows the behavior at the cylinder wall for the predictions using $G_0 = 500kPa$, Case 1. The evolutions of the radial effective stresses ($\Delta\sigma^{'}_{rr}$) with deviatoric strains (ε_d) are plotted in figure 8(a) only for the undrained and drained regimes. In this case the cap model predictions show a more compressible behavior. To characterize the stress path developed during expansion at the cylinder wall, Fig. 8(b) displays the evolution of deviatoric $\sigma_d(r=R) = \sqrt{(\boldsymbol{\sigma} - \frac{1}{3}\mathrm{tr}\boldsymbol{\sigma}) : (\boldsymbol{\sigma} - \frac{1}{3}\mathrm{tr}\boldsymbol{\sigma})}$ and mean effective stresses $\sigma_m{}' = \dfrac{1}{3}\mathrm{tr}\boldsymbol{\sigma}'$. In this space, the clearly difference observed in the undrained stress paths are justified by the different yielding conditions, those yielding conditions affect maximum values of stresses and pore pressure.

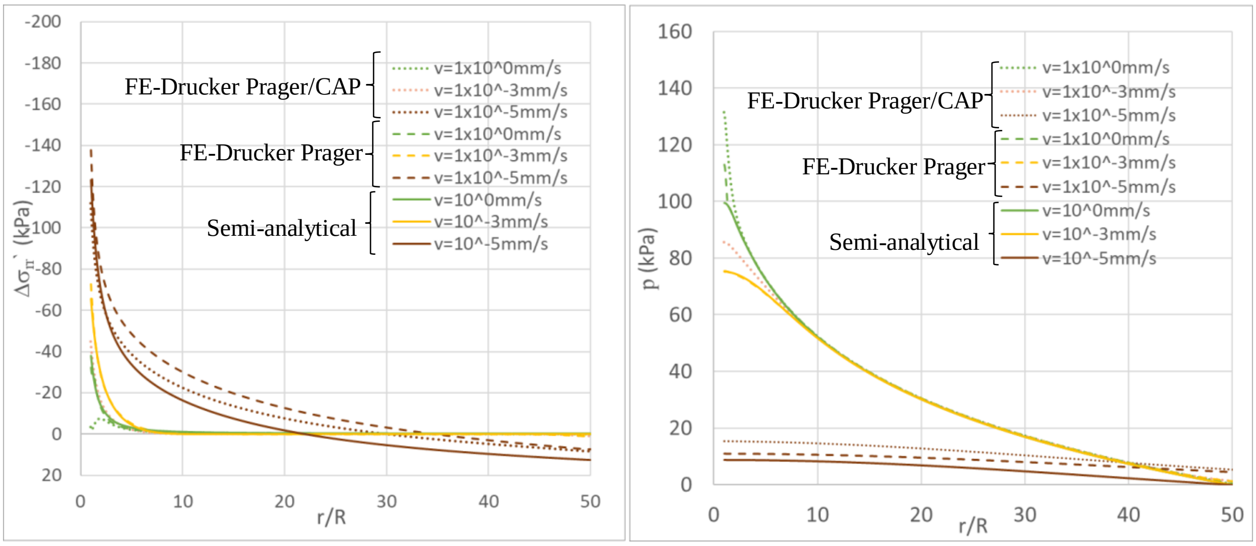

(a) (b)

Figure 7: Distribution of radial stresses and pore-pressure versus radial distance for different expansion rates – G$_0$=500KPa.

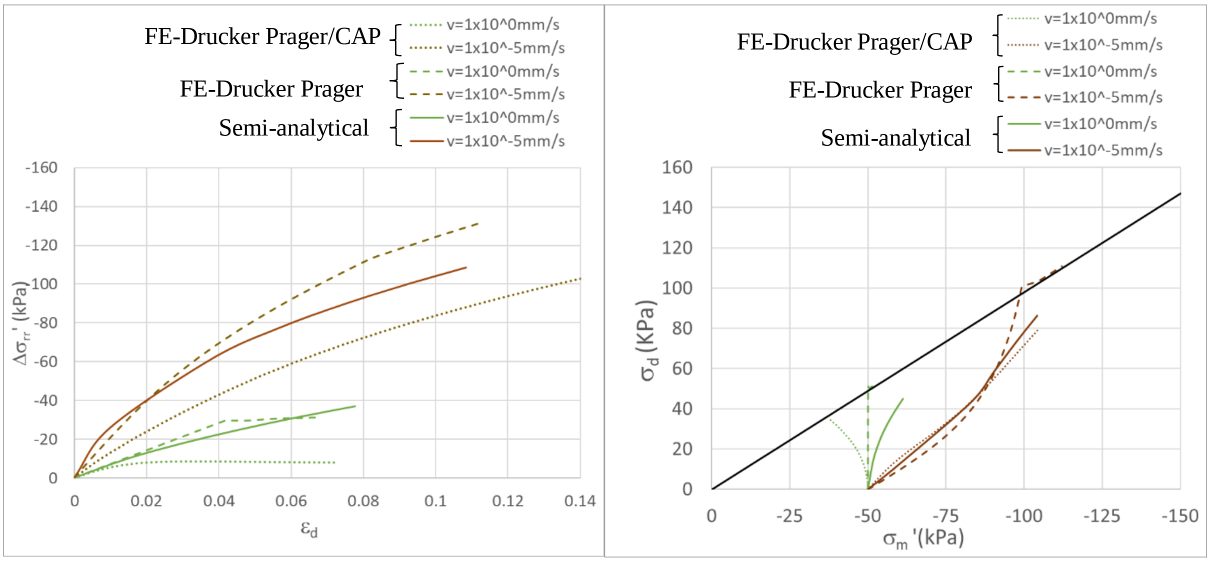

(a) (b)

Figure 8: Radial stresses and Cambridge space for elements adjacent to cylinder wall - G_0=500kPa.

Results at the cylinder wall are reinterpreted to evaluate drained effects during expansion in Figure 9, where a normalized space $V \times U$ is displayed. The normalized space $V \times U$, which correlates the degree of drainage U (Eq. 19), with a normalized velocity V (Eq. 20) is extensively used to determine experimentally rate effects taking place during penetration and rotation of *in situ* tests (House et al, 2001; Schnaid et al, 2004; Randolph & Hope, 2004; Chung et al, 2006; Schneider et al, 2007; DeJong, 2012). In this absence, additional velocities ranging from 10mm/s to 0.00001mm/s are simulated to capture the transitional behavior in Fig. 9. From Fig. 9 we can observe that although the differences pointed previously, there is a good agreement between semi-analytical and F.E. predictions of general drainage behavior. The three models are able to determine the same normalized velocity that characterizes the drained behavior (V≈0.00002). The semi-analytical solution predicts a slighter low value for the undrained minimum normalized velocity (V ≈ 2) compared to that indicated by the F.E. solutions (V ≈ 10).

$$U = 1 - u / u_{0\max} \tag{19}$$

where u is the predicted pore pressure and $u_{0,\max}$ is the initial pore pressure.

$$V = \mathrm{v} \times D / c_f \tag{20}$$

where D is the probe diameter, v the loading rate and c_f (Eq. 21) the coefficient of consolidation

$$c_f = kM \frac{\left(K + \frac{4}{3} G_0\right)}{Mb^2 + \left(K + \frac{4}{3} G_0\right)} \tag{21}$$

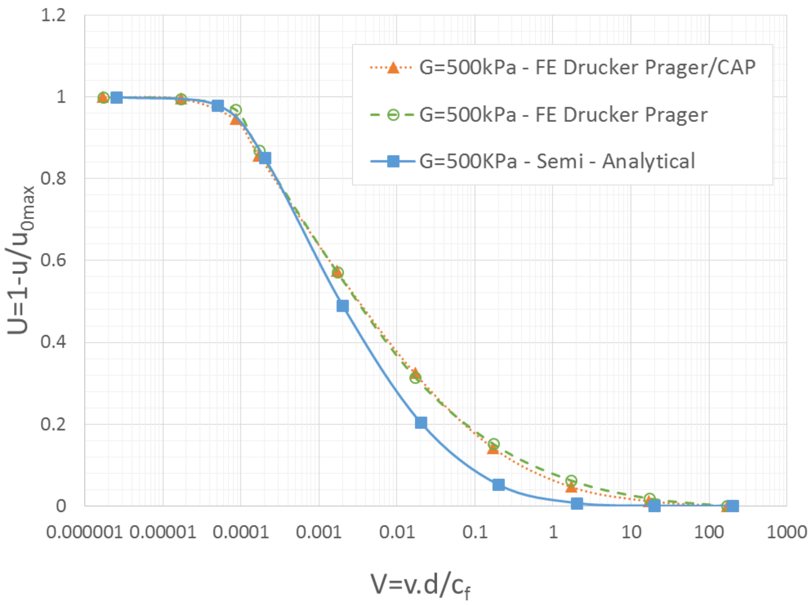

Figure 9: Normalized space V x U – G_0=500kPa.

Results from the second case evaluated, which contemplates a higher initial shear modulus $G_0 = 2500kPa$, are presented in Figures 10 to 12. From Figures 10(a) and 10(b), it is observed, similarly to that described in Case 1, that the maximum effective radial stress ($\Delta\sigma'_{rr}$) and pore pressure (p) are very sensitive to the expansion rate. The non-linear poroelastic model and both poroplastic F.E. solutions predict decreasing values for the maximum stress as the expansion rate increases. F.E. solutions, Drucker Prager and Drucker Prager Cap models, continues predicting higher values of pore pressure, especially at the undrained behavior. A general agreement on $\Delta\sigma'_{rr}$ is observed for the lower velocity (drained). In the partial drained and undrained velocities the F.E. maximum values of $\Delta\sigma'_{rr}$ are sensitively lower, especially for the Drucker Prager Cap model. The same behavior can be observed in Figure 11 (a) which presents the evolution of radial stresses at the cylinder wall. The stress path in Figure 11(b) helps to understand the greater differences observed when G_0 is increased: when G_0 increases, comparing the same applied radial expansion, the shear failure surface is early reached, when the shear failure is reached the yielding behavior domain the final response and the differences between model predictions increase.

To assess the influence in general drainage behavior when higher initial shear modulus is used, results are reinterpreted in $V \times U$ space (Fig. 12). According Fig. 12, the normalized velocity that characterizes the drained behavior is the same as predict for Case 1 (V≈0.00002), showing a good agreement of model predictions. In contrast, the normalized velocity that characterizes the undrained behavior ranges between models from 1 to 10. The differences in the normalized undrained velocity can be a result of the higher values of pore pressure predicted in the F.E. models.

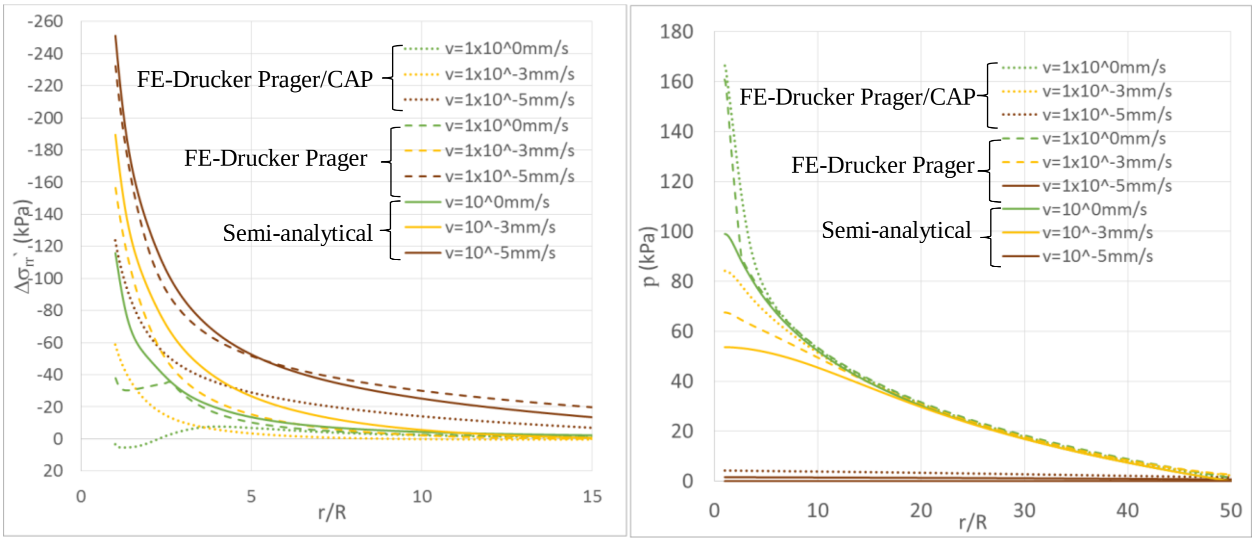

(a) (b)

Figure 10: Distribution of radial stresses and pore-pressure versus radial distance for different expansion rates – G_0=2500KPa.

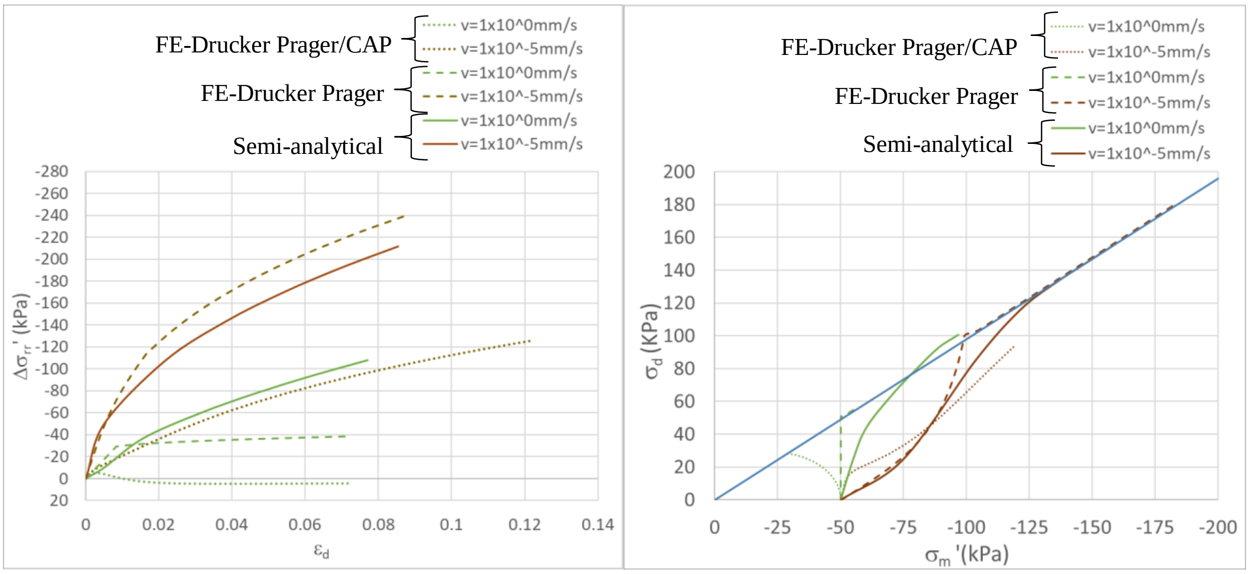

(a) (b)

Figure 11: Radial stresses and Cambridge space for elements adjacent to cylinder wall- G_0=2500kPa.

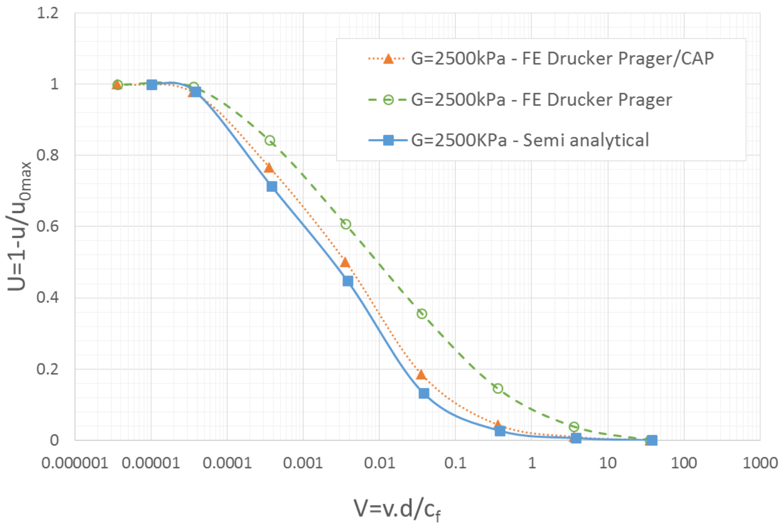

Figure 12: Normalized space V x U – G_0=2500kPa.

4 CONCLUSIONS

Conceived as a simplified approach to flow effects arising in intermediate permeability soils, a non-linear poroelastic model has been formulated and described in Dienstmann et al. (2017) to capture the effects of expansion rate on stress and pore-fluid pressure distributions induced in a porous medium surrounding a rigid expanding cylinder. In the present paper, results of the model predictions are directly compared with poroplastic finite element solutions, using both a Drucker-Prager and Drucker-Prager Cap plasticity models.

The approach application to the cases of frictional-cohesive materials, together with poroplastic F.E simulations, illustrate the ability of the modeling to provide relevant insights into the effects of drainage conditions during cylinder expansion on radial stresses and pore-fluid pressures. The results corroborate the fact that partial consolidation in silty soils can affect shear strength measurements from field tests. In particular, the analysis indicated that maximum mobilized stresses at cylinder wall are very sensitive to expansion rate.

When comparing the different models, the analysis results show that when the shear failure is reached, greater are the differences between the model predictions of stresses and pore pressure, especially looking at the undrained Drucker Prager cap results. This is a direct impact introduced by the yielding cap condition. It is important to highlight that the effects of the cap surface limiting the domain of elastic compressive stresses must be further evaluated. Complementary analyzes varying cap model parameters as R_{DPC} and α_{DPC} would be addressed in future works.

Although the differences evaluated, interpretation of the model predictions in terms of normalized velocity V *versus* degree of drainage U, defines that partially drained behavior occurs at a normalized velocities V in the range of 0.00002 to 10. This range of values can be used for practical recommendations to perform tests at field at different penetration rates in the same location to establish the characteristic drainage curve of the soil to guide interpretation.

ACKNOWLEDGEMENTS

The authors gratefully appreciated the financial support provided by the Brazilian Research Council CNPq.

REFERENCES

Abaqus. *ABAQUS User Manual. Dassault Systèmes*, Simulia Corp. ABAQUS© vs. 6.9, Providence, Rohde Island, USA. 2009.

Baligh, M. M. (1985). "Strain path method." *J. Geotech. Engrg.*, 10.1061 /(ASCE)0733-9410(1985)111:9(1108),1108–1136.

Biot, M.A. (1941). General theory of three-dimensional consolidation. *Journal of Applied Physics*, Vol. 12, pp. 155-164.

Blight, G.E. (1968). A note on field vane testing of silty soils. *Canadian Geotechnical Journal*, Vol. 5, p. 142–149.

Burns, S. E., and Mayne, P. W. (2002). "Analytical cavity expansion – Critical state model for dissipation in fine-grained soils." *Soils Found.*, 42(2),131–137.

Cao, L. F., Teh, C. I., and Chang, M. F. (2001). "Undrained cavity expansion in modified Cam clay. I: Theoretical analysis." *Geotechnique*, 51(4),323–334.

Chang, M. F., Teh, C. I., and Cao, L. F. (2001). "Undrained cavity expansion in modified Cam clay II: Application to the interpretation of the piezocone test." *Geotechnique*,51(4),335–350.

Chen, S.L., and Abousleiman, N.Y. (2012). "Exact undrained elastoplastic solution for cylindrical cavity expansion in modified Cam Clay soil." *Geotechnique*,62(5),447–456.

Chen, S.L., and Abousleiman, N.Y.(2013)."Exact drained solution for cylindrical cavity expansion in modified Cam Clay soil." *Geotechnique*, 63(6),510–517.

Chung, S. F., Randolph, M. F., Schneider, J. A. (2006). "Effect of penetration rate on penetrometer resistance in clay." *Journal of Geotechnical and Geoenvironmental Engineering*, 10.1061/(ASCE)1090-0241(2006)132:9(1188), 1188-1196.

DeJong, J.T. Jaeger, R.A, Boulonger, R.W. Randolph, M.F., Wahl, D.A.J. (2012). Variable penetration rate cone testing for characterization of intermediate soils. *Geotechnical and Geophysical Site Characterization 4*.

Dienstmann, G., Maghous, S., Schnaid, F. (2017). Theoretical analysis and finite element simulation for non-linear poroelastic behavior of cylinder expansion in infinite media under transient pore-fluid flow conditions. *ASCE International Journal of Geomechanics*, 10.1061/(ASCE)GM.1943-5622.0000834.

Gibson,R.E., and Anderson,W.F.(1961)."In situ measurement of soil properties with the pressuremeter." *Civ. Eng. Public Works Rev.*,56,615–618.

House, A.R., Oliveira, J.R.M.S., Randolph, M.F. (2001). Evaluating the coefficient of consolidation using penetration tests. *International Journal of Physical Modelling in Geotechnics*, 1(3): 17-25.

Jamiolkowski, M. and Masella, A., (2014). Geotechnical Characterization of Copper Tailings at Zelazny Most Site. 3rd *International Conference on the Flat Dilatometer*, Rome, Italy.

Lemarchand, E., Ulm, F.J., Dormieux, L. (2002). The effect of inclusions on the friction coefficient of highly-filled composite materials. *Journal of Engineering Mechanics*, 10.1061/(ASCE)0733-9399(2002)128:8(876), 876-884.

Maghous, S., Dormieux, L., Barthelemy, J. (2009). Micromechanical approach to the strength properties of frictional geomaterials. *European Journal of Mechanics, A/Solids*, Vol. 28, 179-188.

Osman, A. S., Randolph, M.F. (2010). Response of a solid infinite cylinder embedded in a poroelastic medium and subjected to a lateral load. *International Journal of Solids and Structures* 47 (2010) 2414–2424

Osman, A.S. (2010). Comparison between Coupled and Uncoupled Consolidation Analysis of a Rigid Sphere in a Porous Elastic Infinite Space. *ASCE Journal of Engineering Mechanics*, 136(8), 1059-1064.

Randolph, M.F., Hope, S.N. (2004). Effect of cone velocity on cone resistance and excess pore pressure. *In: Proceedings of Engineering practice and performance of soft deposits*, Osaka, 147-152.

Randolph, M.F., Wroth, C.P. (1979). An analytical solution for the consolidation around a driven pile. *International Journal for Numerical and Analytical Methods in Geomechanics*, 3(2): 217-229.

Schneider, J.A, Lehane, B.M., Schnaid, F. (2007) Velocity effect of piezocone measurements in normaly and overconsolidation clay. *International Journal of Physical Modelling in Geotechnics*. V 2, p. 23-34

Schnaid, F., Lehane, B. M., Fahey, M. (2004). "In situ test characterization of unusual geomaterials." *Proc., 2nd Int. Conf. on Site Characterization*, Vol. 1, Millpress, Rotterdam, Netherlands, 49–74.

Schnaid, F., Bedin, J., Viana da Fonseca, A. J. P. and de Moura Costa Filho, L. (2013). "Stiffness and Strength Governing the Static Liquefaction of Tailings." *Journal of Geotechnical and Geoenvironmental Engineering*, v. 139, p. 2136-2144.

Teh, C.I. and Houlsby, G.T. (1991). "An analytical study of the cone penetration test in clay". *Geotechnique*, 41(1): 17-34.

Yu, H. S., and Mitchell, J. K. (1998). "Analysis of cone resistance: review of methods." *J. Geotech. Geoenviron. Eng.*, 10.1061/(ASCE)1090 -0241(1998)124:2(140),140–149.

Zhang, Y., Li, J., Liang, F., and Tang, J. (2016). "Interpretation of cone resistance and pore-water pressure in clay with a modified spherical cavity expansion solution." *Bull. Eng. Geol. Environ.*, 75(1), 391–399.